Available online at www.sciencedirect.com
SCIENCE DIRECT®
International Journal of Plasticity 22 (2006) 754–774
INTERNATIONAL JOURNAL OF Plasticity
www.elsevier.com/locate/ijplas

Atomistic based continuum investigation of plastic deformation in nanocrystalline copper

D.H. Warner [a], F. Sansoz [b], J.F. Molinari [a,*]

[a] *Department of Mechanical Engineering, Johns Hopkins University, 104 Latrobe Hall, 3400 North Charles Street, Baltimore, MD 21218, USA*
[b] *Department of Mechanical Engineering, University of Vermont, 33 Colchester Avenue, Burlington, VT 05405, USA*

Received 27 March 2005
Available online 9 August 2005

Abstract

A continuum model of nanocrystalline copper was developed based on results from independent atomistic calculations on 11 bicrystals containing high angle grain boundaries. The relationship between grain boundary structure and its mechanical response was investigated. Based on the atomistic calculations; a constitutive law for grain boundary interfaces was implemented within a finite element calculation that consisted of a microstructure loaded in compression. The yield strength as a function of grain size was compared to experimental data and molecular dynamics results. Calculations were performed to demonstrate the relationship between intragranular plasticity and grain boundary sliding.

Keywords: Nanocrystalline; Finite elements; Quasicontinuum; Grain boundaries

1. Introduction

For several decades the relationship between the plastic behavior of traditional polycrystalline materials and grain size has been well documented, especially with

* Corresponding author. Tel.: +1 410 516 2864; fax: +1 410 516 7254.
E-mail address: molinari@jhu.edu (J.F. Molinari).

0749-6419/$ - see front matter
doi:10.1016/j.ijplas.2005.04.014

respect to deformation modes such as creep (Herring, 1950; Coble, 1963), super-plasticity (Ashby and Verrall, 1973), and dislocation motion (Hall, 1951; Petch, 1953). Recent advances in processing techniques have allowed for the production of dense polycrystalline materials with grain sizes on the order of 10 nm. These nanocrystalline materials have been observed to exhibit different plastic behavior than that predicted by classical theory (Khan et al., 2000; Gertsman et al., 1994; Wang et al., 2003; Hasnaoui et al., 2003; Dalla Torre et al., 2002; Karimpoor et al., 2003; Ebrahimi et al., 1999), most notably deviating from the dislocation based theory of Hall and Petch (Hall, 1951; Petch, 1953). The divergence from the Hall–Petch relationship suggests that there are new deformation mechanisms operating at these small grain sizes.

Direct evidence of different intragranular deformation mechanisms has been obtained for FCC metals with TEM (Chen et al., 2003; Liao et al., 2004). The cause of these partial dislocation emissions from the grain boundaries has been commented extensively (Asaro et al., 2003; Kumar et al., 2003) and has also been observed in molecular dynamics simulations (Schiotz et al., 1998). Nevertheless, simulations predict that intragranular deformation by partial dislocation emissions accounts for only a small portion of the macroscopic deformation, especially at very small grain sizes of $\sim$10 nm, where the existence of any intragranular dislocations is rare or doubted (Legros et al., 2000; Schiotz et al., 1998).

Although very little direct experimental evidence exists (Shan et al., 2004), molecular dynamics (MD) simulations have predicted that the primary mechanism responsible for the plastic deformation in nanocrystalline metals is grain boundary (GB) sliding (Van Swygenhoven and Derlet, 2001; Hasnaoui et al., 2003; Schiotz et al., 1999). Unfortunately, similar to partial dislocation emission from the GB, the mechanics of GB sliding are not well understood.

Recently, several authors have presented grain size dependent; constitutive models for nanocrystalline metals that incorporate GB sliding as the primary mode of deformation (Kim et al., 2001; Conrad and Narayan, 2000; Capolungo et al., 2005). Even though the constitutive behavior at the individual boundaries is soundly derived; these models lack in relating localized GB behavior to the microstructural geometry and the overall macroscopic response.

Although MD has been a useful tool in understanding the localized behavior of nanocrystalline metals, simulations with realistic sample sizes, boundary conditions, and strain rates are outside the scope of MD due to its large computational cost. The hope of carrying out large scale computations that are not bound by the same constraints as MD simulations has prompted several researchers to develop continuum models. Nevertheless, the results obtained from continuum representations must be carefully analyzed because they are contingent on the validity of the constitutive laws used in the model.

In finite element simulations conducted by Fu et al. (2001, 2004) and Schwaiger et al. (2003), the microstructure was modeled as two distinct phases, a grain boundary affected zone (GBAZ), and a grain interior. By decreasing the grain size and consequently increasing the volume fraction of GBAZ, Fu et al. were able to simulate the dependence of yield strength on grain size that has been experimentally observed

in nanocrystalline iron and copper. Shear localization, initiated from grain boundary sliding, was also observed as seen in experiments (Sanders et al., 1997). However, the definition of a GBAZ in these calculations may be questioned. It has been directly observed with TEM (Kumar et al., 2003) that the crystallinity of nanometer sized grains is maintained completely up to the grain boundary with no grain boundary phase observable. Hence, the idea of a large (7 lattice parameters) GBAZ must be based on the assumption that the material in the GBAZ region is different from material in the region further away from the GB. Although the material in the GBAZ may be plastically softer due to the local elastic stress fields from the GB misalignment, it is very difficult to assign a single material property to this region that can describe the combined response of both the grain boundary and the nearby crystal.

The finite element simulations done by Wei and Anand (2004) address this issue by using cohesive elements to describe the GB while describing the intragranular behavior with a classical crystal plasticity model having input parameters corresponding to nanometer sized grains. Both the tensile and shear properties of the cohesive element are determined from experimental fit, which makes it difficult to unambiguously define the GB properties. The shear strength of a GB in their calculations is taken to be the same as the tensile strength. Recent atomistic results of Spearot et al. (2004) and Sansoz and Molinari (2004, 2005), show the tensile strength to be several times stronger than the shear strength.

Based on the TEM observations of Kumar et al. (2003) and following the methodology of Wei and Anand (2004), we have chosen to model nanocrystalline copper using the finite element method with no second phase between grains. Hence our model consists of only the bulk properties of copper and the interfacial properties of the GBs. In order to determine the interfacial properties; the local constitutive response of 11 high angle GB structures were investigated with independent atomistic calculations.

This paper is composed of two distinct sections. The first section describes the atomistic calculations that were performed to examine the behavior of various high angle copper GBs, while the second focuses on finite element simulations of nanocrystalline copper under compression. In both sections, a brief overview of the numerical procedure is given first.

2. Phenomenology of GB sliding at the atomic scale

2.1. Computational procedure and loading configuration

The quasicontinuum method (Shenoy et al., 1999; Tadmor et al., 1996; Miller and Tadmor, 2002) was used to simulate 11 differently structured grain boundaries in bicrystals. By utilizing this technique, a molecular statics solution was obtained without explicitly representing every atom. The regions of the sample that had small deformation gradients were treated as a continuous media using the finite element method. An embedded atom potential given by Foiles et al. (1986) was chosen to

describe the interaction between copper atoms. A typical simulation consisted of less than 8000 representative atoms.

Each bicrystal was constructed using the coincident site lattice (CSL) model. The simulation cell was considered quasi-planar with only one repeated CSL cell along the tilt axis, which was parallel to the [1 1 0] direction. The tilt angle of each grain, which defined the total misorientation angle at the interface, was the angle between the [1 1 0] crystal direction and the normal to the GB plane. Nine ⟨1 1 0⟩ symmetric tilt configurations and two ⟨1 1 0⟩ asymmetric tilt configurations were studied as seen in Table 1. The minimum dimensions of the bicrystal at equilibrium were approximately 400 Å × 100 Å × 5 Å. The simulation cell was relaxed under zero force lattice statics at zero temperature in order to obtain the lowest state of energy for a given GB configuration as detailed elsewhere (Sansoz and Molinari, 2004, 2005).

Simple shear was performed by straining the relaxed bicrystal with a series of incremental shear displacements on the top line of atoms in the upper grain. The atoms on the right and left sides of the cell were free while the bottom and top lines of atoms were fixed in all directions.

The shear stress was calculated by adding the residual forces of the finite element region at the top of the upper grain and dividing by the GB area. The current procedure can be interpreted as an estimate of the average "far-field" stress without the need for the calculation of local stress variations across the boundary. Despite the approximation made on the stress definition, Sansoz and Molinari (2004, 2005) have shown in an earlier investigation that the calculated stress is in excellent agreement with the average stress obtained in molecular dynamics studies of single crystals (Horstemeyer et al., 2003; Roundy et al., 1999) or bicrystals (Spearot et al., 2004).

2.2. GB strength and deformation mechanisms

In shear, the 11 different GB structures deformed by one of the three following mechanisms: shuffling; migration, and partial dislocation nucleation. The shear

Table 1
Constitutive parameters of copper ⟨1 1 0⟩ tilt grain boundaries under shear

Type	(*hkl*) GB plane	Misorientation angle (°)	Energy (mJ/m^2)	τ^0_{crit} (GPa)	Deformation mode
STGB	Σ27(552)	31.58	870	2.07	GB shuffling and partial nucleation
	Σ33(441)	20.04	863	1.90	GB shuffling only
	Σ9(221)	38.94	833	1.39	GB shuffling and partial nucleation
	Σ11(332)	50.48	699	1.68	GB shuffling and partial nucleation
	Σ27(115)	148.4	699	2.96	GB migration
	Σ73(661)	13.44	674	1.03	GB migration
	Σ33(554)	59.00	488	1.61	Dissociated stacking faults from GB
	Σ11(113)	129.52	309	5.41	Partial nucleation from GB
	Σ3(111)	70.52	9	2.35	Twin migration
ATGB	Σ11(225)/(441)	39.52	680	3.08	Dissociated stacking faults from GB
	Σ121(110)/(7712)	39.52	701	1.55	GB shuffling only

STGB, symmetric tilt grain boundary; ATGB, asymmetric tilt grain boundary.

deformation mechanisms with respect to GB structure are summarized in Table 1. Additionally, Table 1 gives the level of shear stress, τ^0_{crit}, necessary to induce plastic behavior within the bicrystal system at 0 K.

The stress strain relationship associated with GB shuffling is shown in Fig. 1. During GB shuffling, the behavior of a few GB atoms was uncorrelated with the reminder of the bicrystal, where atoms were homogeneously shifted parallel to the interface (Fig. 2(a)). For clarity, we circled the regions of atomic shuffling. Fig. 2(b) shows that a specific point defect, also circled, was the site for the nucleation and propagation of a partial dislocation. The emitted partial dislocation is depicted with the bright-colored atoms.

For some of the GB configurations shown in Table 1, plastic deformation occurred by a collective atom migration of the interface perpendicular to the loading direction. In this process, the interface migrated discontinuously as shear was applied, i.e., the bicrystal deformed elastically up to the level of stress τ^0_{crit}, which subsequently lead to sudden GB migration. For the $\Sigma 33(554)$ symmetric GB, which was initially dissociated into extended stacking faults after equilibrium, it was found that the dissociated faults propagate in the crystal, and neither shuffling nor migration processes occurred in this case.

In summary, it was found that GB sliding occurred at stress levels between 1.4 and 2.1 GPa at 0 K. In some cases, GB shuffling was accompanied by partial dislocation emission and in other cases plastic accommodation was solely due to GB migration. The simple shear behavior of a sliding GB is reminiscent to a stick-slip process: which differs from a cleavage-like GB fracture. As shear strains increase, elastic

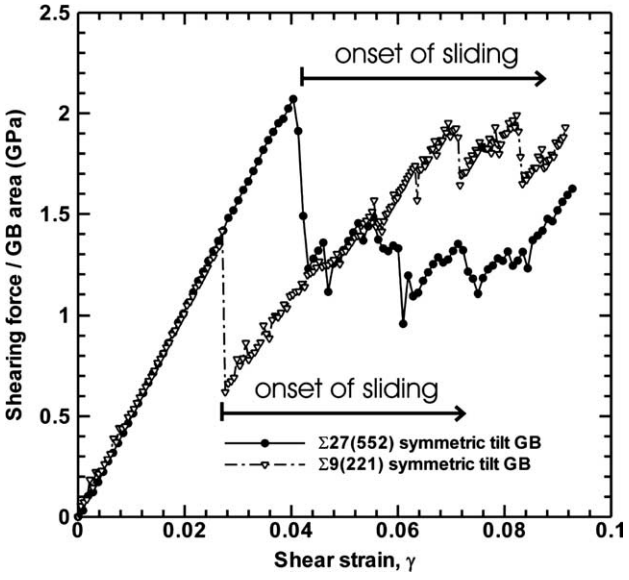

Fig. 1. Evolution of the shear stress acting on the cell as a function of the applied shear strain for two ⟨1 1 0⟩ symmetric tilt GBs. For both GBs, the onset of GB sliding starts as indicated.

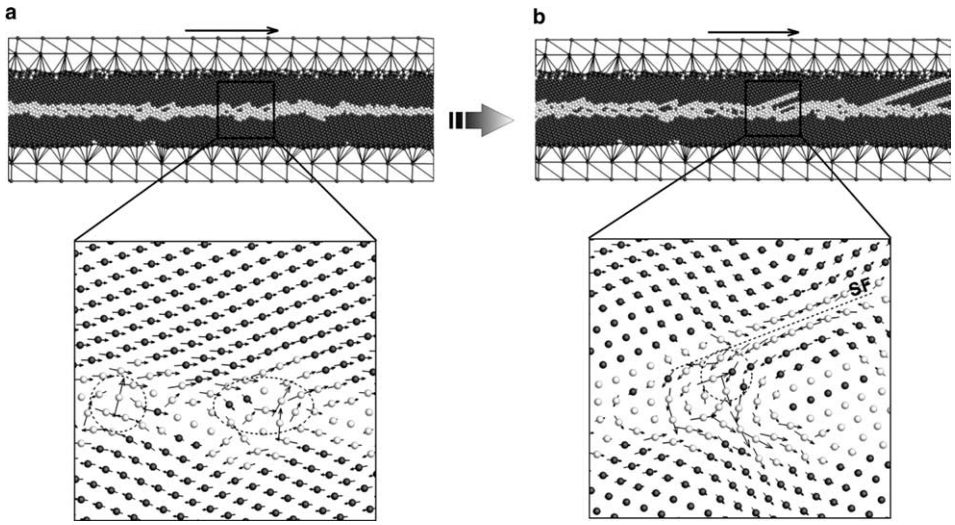

Fig. 2. Deformation mechanisms of a Σ27(552) symmetric tilt GB under shear. (a) Early stage of GB sliding initiated by localized shuffling events (dashed circles) of atoms at the interface. Arrows correspond to the atomic displacement between two loading steps. Note that the motion of some atoms at the interface is uncorrelated to the displacement of the crystal lattice (dark atoms). (b) Subsequent stage of GB sliding where sites of atomic shuffling in the GB nucleate partial dislocations traveling into the grain and leaving a stacking fault (SF).

strains build up until a maximum stress is reached; thereby leading to a new GB configuration. This new configuration is obtained by atomic shuffling of the interface through the mechanism described above. This information will be used in Section 3.3 for the development of a constitutive law to describe GB behavior in the finite element simulations.

2.3. Correlation between GB structure and sliding

A direct correlation was found to exist between GB sliding and the presence of a particular point defect in the GB. The GBs containing the defect necessary for sliding were high energy GBs but not all high energy GBs contained the particular point defect necessary for GB sliding. Thus, the high energy of a GB seems to be necessary for triggering GB sliding but it is not a sufficient parameter, as observed in the experimental studies of Hanyu et al. (2004). Examples of this can be found in Table 1.

No direct correlation between the density of the particular point defect necessary for GB sliding and the GB sliding strength was obtained. This result suggests that a local analysis of the stress distribution along the interface would be a better way to interpret the change in mechanical strength between different GB configurations. It is worth pointing out once more that not all GB structures lead to sliding, for which case the mechanisms of GB migration or nucleation of partial dislocations from the GB are favored. Finally, it is concluded that there is no simple way of relating

GB energy or misorientation angle to constitutive response within the finite element calculations.

3. Finite element simulation of nanocrystalline copper

The remainder of this paper will focus on the implementation and interpretation of the finite element calculations on nanocrystalline copper. The constitutive laws put into the model were inspired from the atomistic calculations described in Section 2. along with the current theoretical and experimental understanding of this material.

3.1. Computational framework

The finite element analysis was performed within a Lagrangian framework using an explicit dynamic methodology (Hughes, 1987). A standard six node triangular element was used to discretize the 2D Cartesian configuration space. Time integration was lumped into two distinct parts. First, integration of the equations of motion was performed without regard to the kinematic constraints imposed by the GB interfaces. Second, a correction of the kinematic variables was applied to account for contact and adhesion between bodies.

The discretize equations of motion for each node at time $t_{n+1} = t_n + \Delta t$ were determined using a modified central difference scheme where Δt was chosen to be a fraction of $h/\sqrt{C_{44}/\rho}$, which was sufficiently less than the numerical stability limit (Bathe and Wilson, 1976), where ρ and h correspond to the density and minimum element size, respectively. Thus, the unconstrained displacements $\hat{u}_{n+1}$, accelerations $\hat{a}_{n+1}$, and velocities $\hat{v}_{n+1}$ at time n, were calculated using the following algorithm:

$$\hat{a}_n = \frac{f_n}{M}, \tag{1}$$

$$\hat{v}_{n+1} = \hat{v}_n + \hat{a}_n \Delta t, \tag{2}$$

$$\hat{u}_{n+1} = \hat{u}_n + \hat{v}_{n+1} \Delta t \tag{3}$$

with M representing the lumped mass matrix and f_n being the residual force vector, which was calculated at the element level.

The explicit dynamic method of time integration was chosen due to its ease of implementation; specifically with respect to the interfacial forces and the evolution of plastic strain within the crystal plasticity framework. Application of the explicit dynamic method to quasi-static conditions required a very small loading rate, which is computationally expensive. In order to improve the efficiency, a small amount of numerical velocity dissipation was applied at regular time intervals so that loading could take place at higher rates without the influence of inertial effects.

Due to the compressive state of stress, the enforcement of contact and adhesion between grains was the most challenging part of the numerical calculations both with respect to computational expense and implementation. However, in order to remain

true to the objective of this paper, the reader should refer to a separate work (Warner and Molinari, to be submitted) for a detailed account of the algorithm.

3.2. Constitutive model for grain interior

The modeling of the grain interior was carried out using a classical rate-dependent crystal plasticity model. The incremental deformation kinematic equations follow Anand and Kothari (1996), while the plastic slip rate, $\dot{\gamma}^{\alpha}$, on each slip system, α, was calculated using the rate-dependent law developed by Asaro and Needleman (1985),

$$\dot{\gamma}^{\alpha} = \dot{\gamma}_0 \left| \frac{\tau^{\alpha}}{g^{\alpha}} \right|^{\frac{1}{m}} \operatorname{sign}(\tau^{\alpha}), \tag{4}$$

where $\dot{\gamma}_0$, τ^{α}, and g^{α} are the reference shearing rate, critical resolved shear stress on the slip system α, and the slip system deformation resistance, respectively. The parameters, m and $\dot{\gamma}_0$, characterizing the rate sensitivity, were chosen to be 0.01 and 1.0, respectively. These values were chosen so as to minimize the rate sensitivity while ensuring numerical stability of the calculation under the given loading conditions.

Because the application of this model is to nanocrystalline copper ($D < 50$ nm), g^{α} was assumed to remain constant throughout the calculations, i.e., no strain hardening. This assumption is based on the idea that most dislocations in nanosized grains arc emitted from the GB and travel very quickly across the grain to be absorbed by a neighboring GB (Kumar et al., 2003). Therefore, the intragranular strain hardening could only result from changes in the case of nucleation and absorption of dislocations in the GB, which has not yet been quantified.

The value of g^{α} was roughly estimated in each grain as

$$g^{\alpha} = \frac{Gb}{D} \tag{5}$$

with G representing the shear modulus, b the Burgers vector, and D the grain diameter (Asaro et al., 2003; Wei and Anand, 2004). For all grain sizes, the value of g^{α} was limited to be less than the theoretical critical shear stress of 1.0 GPa in the $\langle 1\ 1\ 2 \rangle$ direction as determined from density functional theory calculations performed by Roundy et al. (1999).

The elastic stiffness coefficients corresponding to single crystalline copper were chosen as $C_{11} = 168.4$ MPa, $C_{12} = 121.4$ MPa, and $C_{44} = 75.4$ MPa.

At this point, it is critical to point out the short comings of this intragranular model. First, there is evidence (Asaro et al., 2003; Chen et al., 2003; Liao et al., 2004) that partial dislocation emission in copper is energetically favored compared to full dislocation emission at these small grain sizes. Secondly, atomistic calculations (Sansoz and Molinari, 2004, 2005; Van Swygenhoven and Derlet, 2001) suggest a link between GB sliding and partial dislocation emission which is not included in this work. Finally, the use of a continuum model at such small length scales docs not accurately represent the physics associated with dislocation motion. For instance,

one dislocation traveling across a 10 nm grain induces a plastic strain of ~4%. This type of discrete behavior obviously cannot be modeled within the crystal plasticity framework presented here. Despite, all of these shortcomings, it is believed that the crystal plasticity model used here can act as an approximation to the anisotropic plastic deformation that occurs inside of nano-grains and, therefore, can be qualitatively used to gain a better understanding of the deformation characteristics of nanocrystalline metals.

3.3. Grain boundary constitutive model

The application of the stress–strain data, obtained in the atomistic calculations, to cohesive laws that are suitable for use within a finite element simulation must be done with care. The results given in the atomistic section of this paper describe the response of a bicrystal which deforms both elastically within the grains and plastically at the interface. Thus, the elastic part of the atomistic calculations must be subtracted from the stress–strain curves in order to obtain an accurate cohesive law for the interface in the finite element calculations. This issue has been comprehensively addressed by Rice (1992) and Nguyen and Ortiz (2002). Following the work of these authors, Eq. (6) was used to estimate the adhesive properties of GBs. The adhesive stress at a GB, σ^{adhesive}, was given as a function of the separation distance, δ as

$$\sigma^{\text{adhesive}} = \sigma_{\text{crit}}\left(1 - \frac{\delta}{\delta_{\text{crit}}}\right), \tag{6}$$

where σ_{crit} is the adhesive strength of the interface and δ_{crit} is the critical opening displacement at which adhesive forces are no longer felt. In typical uses of this cohesive model, δ_{crit} is usually chosen to account for the energy dissipation related to the debonding of two surfaces. However, in the present model δ_{crit} has been chosen to be equal to 1 nm to ensure numerical stability at moderate time steps and attempt to capture the characteristics of interfacial decohesion at the atomic scale. It should be noted that in this representation of GBs, the locally reduced elastic modulus of the GB is not included. The effect of this approximation is negligible down to extremely small grain sizes due to the atomistically sharp nature of the GBs considered in this work Sansoz and Molinari (2004).

A value of 2.4 GPa was chosen for σ_{crit}. This value has been suggested by Rice and Beltz (1994) for the decohesion of two planes copper atoms at room temperature. The value is in line with the results obtained through our own, in-house, thermally corrected, atomistic calculations of the tensile strength of GBs (~2.0 GPa) at room temperature. Through atomistic calculations similar to those done in the earlier section, which were not presented here for brevity, it was determined that the tensile strength of GBs can be approximated as roughly independent of GB structure. Accordingly, all high angle GBs in the finite element calculations were assigned the same adhesive properties.

From the atomistic calculations in Section 2, the maximum shear strength of the GBs that slid was found to vary from 1.4 to 2.1 GPa, at 0 K, depending on the GB

structure. Based on those results, several approximations were necessary to apply the atomistic results to constitutive laws used in the finite element calculation.

The first approximation was that the shear strength, τ_{crit}, of all GBs was assumed to be constant with shear displacement. This assumption was based on the atomistic results that show GB shear strength depends on the specific atomic structure of the GB and that during plastic deformation the atomic structure is constantly changing. Thus, the shear strength of a GB can go through periods of softening and hardening as plastic deformation progresses. For this reason, an averaging assumption of constant GB resistance to shear is made. Although this assumption may not apply for large strains where some damage may occur at the GB, the assumption of no softening or hardening is reasonable for the magnitude of GB shear strains that occur in this model.

The second major assumption was that GB shear and tensile strengths were uncoupled. Although there is undoubtedly a coupling between shear and tensile strengths, to the best of the authors' knowledge, there is no available data on this subject. While this constitutes a worthwhile topic for future research, in this study the coupling between shear strength and tensile stress was neglected. This reflects that the atomistic contact area between grains is likely to remain constant over a wide range of tensile stresses.

Third, because GB energy and orientation angle were not found to be sufficient parameters to determine if sliding would occur, the shear strength of high angle GBs in the finite element calculations were assigned randomly following a uniform distribution.

Finally, a thermal correction was applied to the 0 K molecular static results. Whether performing molecular dynamics or statics, the atomistically calculated constitutive relationships consist of much higher stresses than experimentally observed due to the high strain rate or zero temperature associated with the respective atomistic calculation methods. Furthermore, if the high stress levels from the atomistic calculations are used directly in the finite element constitutive laws, the qualitative behavior of the finite element simulation becomes unrealistic due to the large amounts of strain energy in the system. Thus, while it is acknowledged that applying a thermal correction to molecular statics is an ad hoc but necessary approximation, it is believed that the conclusions reached in this work are not affected by this estimation.

Assuming that thermally activated GB sliding is controlled by localized atomic shuffling within the point defect responsible for GB sliding, the activation volume, V, associated with GB sliding was estimated as $7b^3$. It is noted that this value agrees with macroscopic values of activation volume in nanocrystalline metals, which is on the order of $10b^3$ (Wei et al., 2004). Thus, the GB shear strength; τ_{crit}, at room temperature; T, was found by solving

$$\dot{\gamma}_{gb} = \gamma_0 \nu \exp\left(\frac{V(\tau_{crit} - \tau^0_{crit})}{TK}\right), \tag{7}$$

where γ_0 represents the average shear strain per successful thermal fluctuation at the grain boundary, ν the Debye frequency. K the Boltzmann constant and τ^0_{crit} the shear strength of the GB at 0 K. In order to mimic quasi-static experimental conditions,

Eq. (7) was solved with $\dot{\gamma}_{gb} = 10^{-3}\ s^{-1}$ and $v = 10^{13}\ s^{-1}$. The localized shear strain at the GB per successful thermal fluctuation was estimated from the atomistic calculations to be 0.5, which gave the relationship

$$\tau_{crit} = \tau^{0}_{crit} - 1.34\ \text{GPa}. \tag{8}$$

Although the use of Eq. (7) is questionable when applied to such a large thermal correction, it is noted that the results are in line with previous MD studies by Schiotz et al. (1999) that suggest the flow stress is 1.2 GPa lower at room temperature than 0 K in nanocrystalline copper. Furthermore, a similar equation to Eq. (7) has been effectively used by Conrad and Narayan (2000) for investigation of GB mechanical properties.

3.4. Microstructure and loading conditions

All calculations performed in this study were conducted on the same topological microstructure. Changes in grain size were carried out by multiplying the coordinates of the microstructure by a scalar. The microstructure consisted of 200 grains created from Voronoi tessellation and was meshed using 14,866 elements. A log–normal distribution of grain size was obtained by manipulating the placement of the tessellation seeds while using a Monte-Carlo approach (Gross and Li, 2002). The orientation of each grain was assigned at random following a uniform distribution within 3D orientation space.

The microstructure was loaded in compression in the vertical direction by application of a displacement on the top nodes at a strain rate low enough to negate inertial dynamic effects so as to mimic quasi-static loading conditions (Fig. 3). The bottom of the square microstructure was fixed in the loading direction with both sides remaining free.

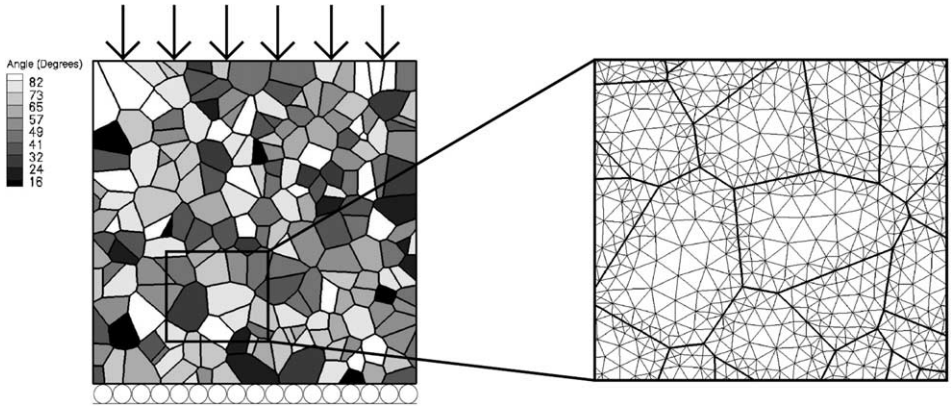

Fig. 3. View of the loading conditions, microstructure, and mesh used in this work. The contour color represents the angle between the ⟨0 1 0⟩ family of directions (projected onto the *xy* plane) and the loading axis.

4. Results and discussion

4.1. Grain size dependence of yield strength

The stress–strain curves for simulations having various grain sizes are presented in Fig. 4. All samples were loaded until large distortions in the mesh required the calculation to be stopped. Therefore, the ending of a stress–strain curve did not necessarily constitute catastrophic material failure.

A clear dependence on grain size was observed with respect to both the magnitude and the shape of the stress–strain curves. Before softening began, and specifically with respect to the smaller grain sizes, these shapes were qualitatively similar to those observed in experiments by Youngdahl et al. (1997).

The premature softening at 2.5% strain, in the 5 and 10 nm grain sizes is thought to result from the effect of the free boundaries being amplified by the small number of grains in the calculation. Furthermore, the early onset of softening may also result from the lack of an accommodation mechanism such as diffusion or microstructural rearrangement that would help to relax the geometrical constraints at triple junctions that hinder GB sliding in the finite element model.

A comparison of the finite element calculations with results from MD and experiments was conducted in order to gain insight into the deformation mechanisms associated with nanocrystalline copper. It is necessary to point out that comparison of the values plotted in Fig. 5 must be done with care for reasons that will be stated throughout the following discussion. First, it is noted that the representative experimental results shown in Fig. 5 for nanocrystalline copper, by Youngdahl et al.

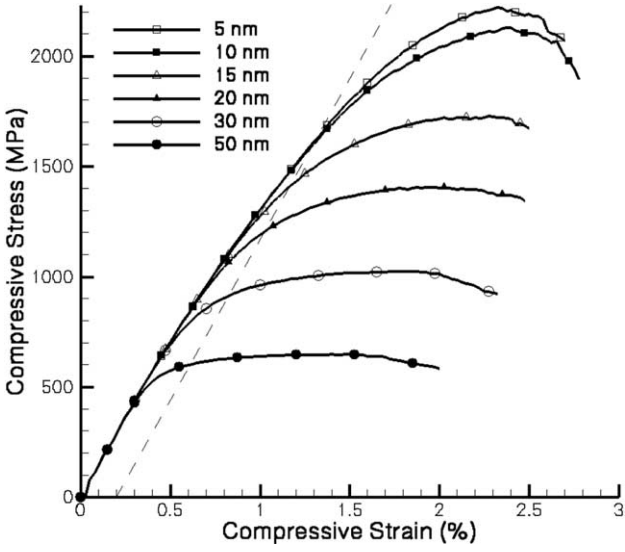

Fig. 4. Calculated stress–strain curves for different grain sizes of nanocrystalline copper loaded in quasi-static compression at room temperature.

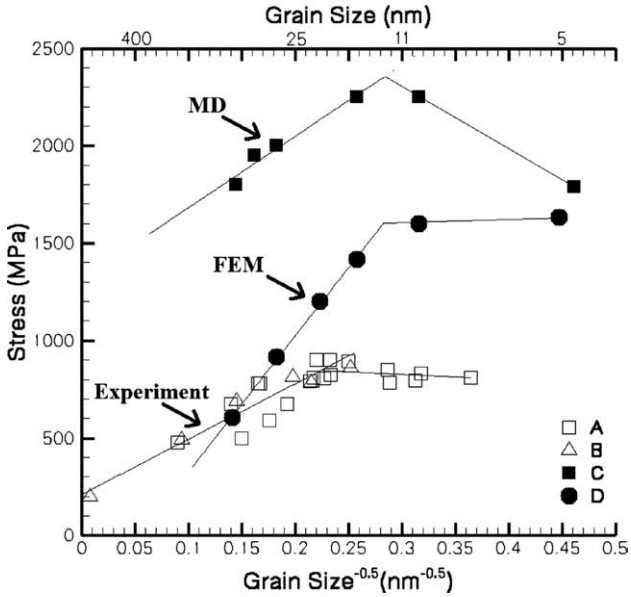

Fig. 5. Comparison the strength versus grain size for nanocrystalline copper: A – hardness divided by 3, Sanders et al. (1997); B – hardness divided by 3, Youngdahl et al. (1997); C – flow stress from MD, Schiotz and Jacobsen (2003); D – yield stress at 0.2% offset strain as measured in the present finite element calculations.

(1997) and Sanders et al. (1997), are values of the hardness divided by 3, which only give an empirical estimation of the yield stresses at 0.2% offset strain (assuming limited hardening).

The finite element data presented in Fig. 5 represent the yield stress as determined by the average stress measured at the base of the sample and recorded at 0.2% offset strain. With that being said, the most obvious difference between the finite element results and those seen in experiment was the difference in yield stresses. For the most part, the higher stress levels in the finite element calculations throughout the paper are not thought to result from inaccuracies in the values chosen for the constitutive laws. Accordingly, it is believed that the high stress levels obtained in the finite element calculations result from the contribution of two separate effects. First, there are deformation mechanisms present in experiment that were not included in the finite element calculations (diffusion, GB migration, partial dislocations, etc.). Second, the finite element calculations were conducted in 2D plain strain, which by definition leads to a stiffer elastic modulus and a possibly higher uniaxial yield strength. Additionally, a back of the envelope calculation reveals that the ratio of grain boundary surface over grain volume increases 50% when going from a 2D to 3D simulation. This large increase is likely to result in more favorable sliding paths and thus decreased stress levels.

The MD results from Schiotz and Jacobsen (2003) that are presented in Fig. 5 demonstrate stronger strengths than both the finite element calculations and exper-

iments. This is most likely due to several factors, one of which being that the values plotted in Fig. 5 represent flow stress not yield stress. In order to obtain a useful comparison of strength versus grain size, Schiotz and Jacobson were required to compare the flow stress rather than the yield stress due to the very high strain rates ($\sim 10^8\ s^{-1}$) at which their calculations were carried out. Furthermore, it must be remembered that the high strain rates may be responsible for the operation (or inoperation) of deformation mechanisms which may (or may not) occur at experimental strain rates. The operation of different deformation mechanisms, such as shear localization, may also be further inhibited by the periodic boundary conditions. Nevertheless, if one assumes that no relaxation or diffusion based mechanisms are operative in the MD calculations, then they can roughly be thought of as operating by the same basic deformation mechanisms as the finite element calculations. Thus, it is encouraging that the maximum flow stress measured in MD (2.3 GPa) is similar to the maximum flow stress obtained in the finite element calculations (2.2 GPa), considering that the finite element calculations were hierarchically developed without any explicit parameter fitting.

A Hall–Petch behavior was qualitatively observed in all three of the data sets at grain sizes greater than 15 nm. Even though the grain size dependence in the finite element calculations scaled as D^{-1}, an almost linear relationship was observed when plotted against $D^{-0.5}$ for the small range of grain sizes considered. The slope of the Hall–Petch relationship in the finite element calculations was found to be noticeably steeper than observed in experiment and MD. This was a result of partial dislocations not being included into the crystal plasticity model. If partial dislocations were included, the stress dependence on grain size in Eq. (5) would be less by a factor of $1/\sqrt{3}$ due to the smaller Burgers vector associated with partial dislocations. By applying this factor to the finite element data, general agreement between the Hall–Petch slopes of the experimental, MD, and finite element results may be obtained.

The negative Hall–Petch slope seen in the MD calculations for very small grain sizes was not observed in the finite element model and is sometimes thought to be an artifact of sample preparation in experimental results. The fact that it was not observed in the finite element model suggests that it is not a result of GB sliding alone, and is perhaps an effect of increased GB volume fraction, GB migration or some other mechanism that is operative at high strain rates and was not included in the finite element model. It is important to point out that this conclusion is not believed to be an artifact of the 2D representation. Considering the current GB deformation mechanisms included in the model, the increased ratio of grain boundary to grain interior in 3D compared to 2D would not lead to a negative Hall–Petch slope in the smallest grain sizes. However, a 2D representation would affect the shape of the Hall–Petch plot if additional GB deformation mechanisms were included; such as those that depend on GB volume fraction (i.e., diffusion).

4.2. Analysis of GB based deformation

One of the benefits of a continuum model is that the extent of participation of each deformation mechanism is readily available. By plotting the amount of plastic

dissipation due to GB sliding compared to the total amount of plastic dissipation resulting from both GB sliding and intragranular plasticity (Fig. 6), a transition in deformation mechanisms with respect to grain size can be observed. GB sliding was evident in all grain sizes modeled. This corresponded well with the MD results

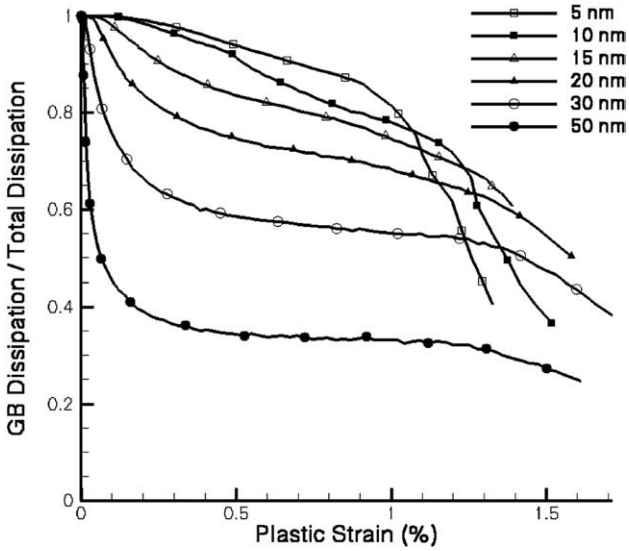

Fig. 6. Comparison of the plastic dissipation due to GB sliding versus the total plastic dissipation due to both GB sliding and intragranular plasticity for different grain sizes.

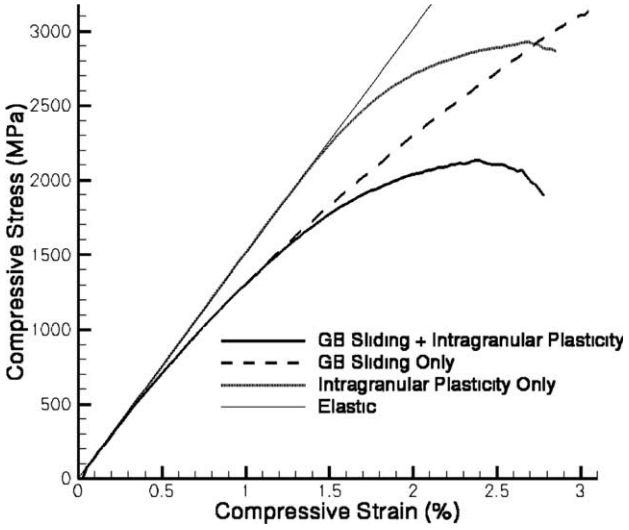

Fig. 7. Stress–strain response of 10 nm nanocrystalline copper having different deformation mechanisms.

of Schiotz and Jacobsen (2003) who observed GB siding at grain sizes up to 49 nm. The continuum model also shows intragranular plasticity occurring at all grain sizes, although this may be an artifact of the continuum crystal plasticity model used. The sharp increase in the amount of intragranular plasticity in the 5 and 10 nm samples near the end of their respective calculations corresponds to the localization of deformation to isolated pockets of a few grains. This is due to the intragranular constitu-

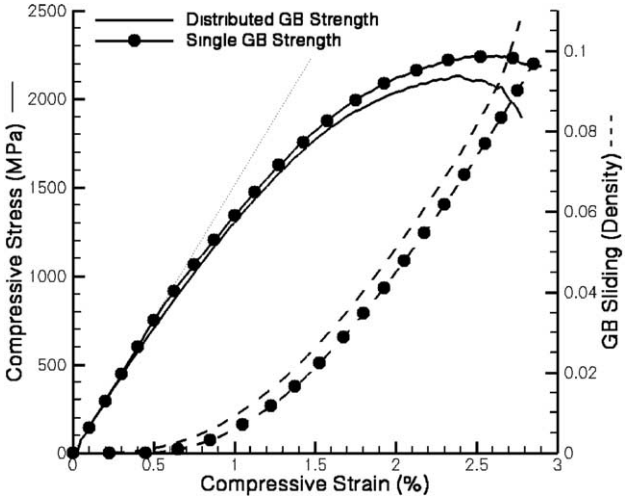

Fig. 8. Comparison of 10 nm nanocrystalline copper having distributed GB shear strength versus non-distributed. GB sliding plotted with the respective stress–strain curves.

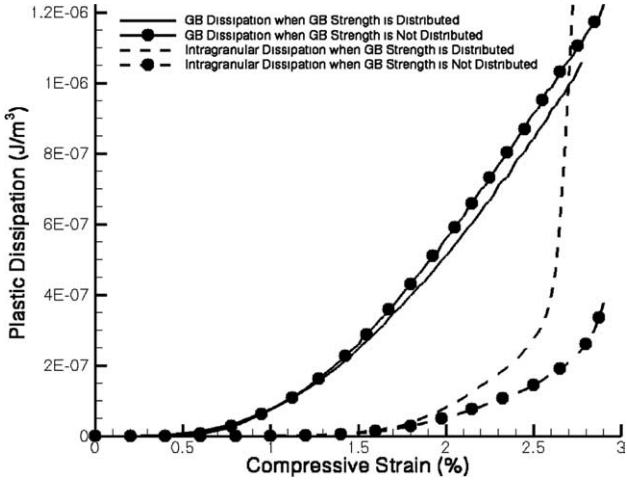

Fig. 9. Comparison of 10 nm nanocrystalline copper having distributed GB shear strength versus non-distributed. Plastic dissipation due to GB sliding and intragranular plasticity plotted versus strain.

tive law having no hardening (i.e., no dislocation–dislocation interactions or exhaustion of GB sources).

In order to gain an understanding of the relationship between GB sliding and intragranular deformation, calculations were performed where only a single deformation mechanism was permitted (Fig. 7). These calculations were carried out on the microstructure having an average grain size of 10 nm. Higher peak stresses were obtained when each mechanism was isolated compared to when both GB sliding and intragranular plasticity were allowed to participate. The lower stress levels, when both mechanisms were allowed, was attributed to the occurrence of intragranular plasticity at smaller macroscopic strains. The decreased stress, at which the intra-

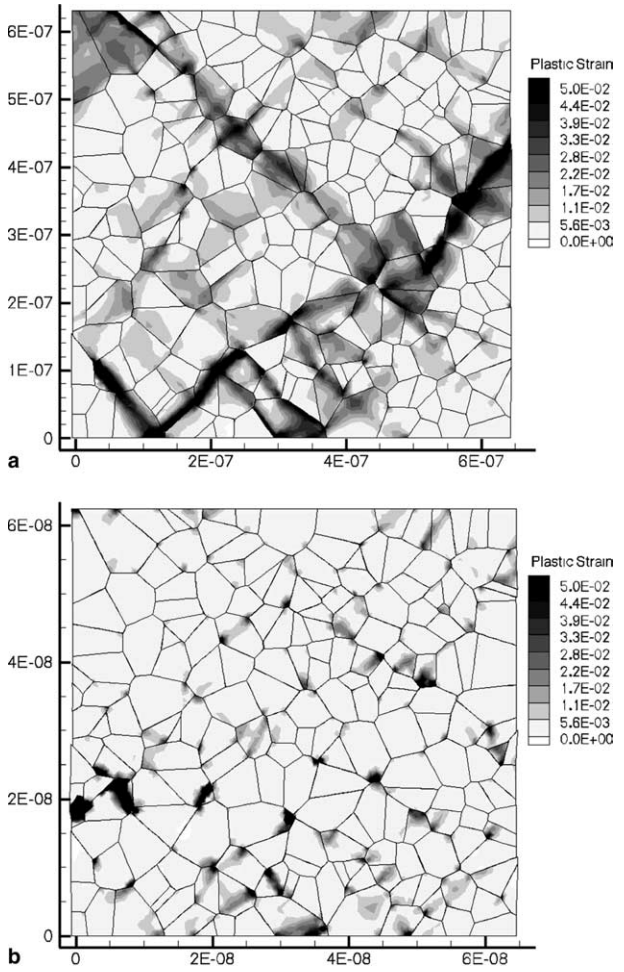

Fig. 10. Plot of the equivalent plastic strain measured at a macroscopic plastic strain of 1.0%: (a) 50 nm grains; (b) 5 nm grains.

granular plasticity occurred, resulted from an increase in the stress heterogeneity which was the consequence of GB sliding. Indeed, the locally decreased shear stress at which GBs slid, resulted in a significant portion of the load being transferred to the geometrically constrained triple junctions. The high stress at these triple junctions created additional GB sliding and intragranular plasticity.

To further investigate the effect of GB sliding, an additional calculation was conducted. In this calculation, all high angle GBs were assigned the same shear strength so as to have the same total shear strength per unit length as the original calculation with a 10 nm average grain size. Fig. 8 shows a comparison of the stress–strain response of the two calculations. The calculation with the distributed GB shear strength was weaker than the one with a single GB shear strength. This is a direct result of weak GBs sliding earlier and therefore leading to further GB sliding, which ultimately resulted in a decrease in the overall strength of the microstructure.

The idea that GB sliding promotes intragranular plasticity can also be seen by plotting the amount of intragranular plastic dissipation versus strain for the two previous calculations (Fig. 9). As expected, the sample with greater amounts of GB sliding had larger amounts of intragranular plastic dissipation due to the increased stress heterogeneities resulting from GB sliding. Thus, it seems that dislocation nucleation from GBs in nanocrystalline metals results indirectly from the high stress levels created from GB sliding as shown in this work and directly from the atomistic shuffling associated with GB sliding as shown in Section 2.

In addition to GB sliding creating increased amounts of stress heterogeneity, it was also observed to dramatically change the way in which plastic deformation localized within the microstructure. Fig. 10 shows the equivalent plastic strain in the 50 and 5 nm calculations measured at a macroscopic plastic strain of 1.0%. The deformation was localized into bands at angles close to 45° in the 50 nm case. The 5 nm case was obviously different as the localization had not yet formed into bands and was concentrated at the junctions of grains.

5. Conclusion

By using a continuum model to investigate the deformation of nanocrystalline copper, we have been able to investigate the interaction between GB sliding and intragranular plasticity. Without any explicit parameter fitting, the finite element model captured many of the qualitative characteristics associated with nanocrystalline metals. By comparison with experimental results, the importance of additional deformation mechanisms that were not included in the model (diffusion, GB migration, etc.) are evident. Further comparison to MD results suggests that a negative Hall–Petch could not result from GB sliding alone but would most likely be the result of the increasing GB volume fraction or a stress activated deformation mechanism such as GB migration that was not included in our model. Additionally, the finite element model used in this work suggests that the D^{-1} relationship is well suited for describing intragranular deformation in the 15–50 nm range when partial dislocations are considered active.

GB sliding was shown to create higher stress heterogeneities, which induced further GB sliding and intragranular plastic deformation. This indicates that reducing the width of GB strength distribution in a microstructure increases its strength. Differences in the extent of plastic localization were also observed at different grain sizes for the same amount of macroscopic plastic strain, these differences would most likely lead to different failure mechanisms and should be further studied in order to improve the characteristics of these materials.

Future work will consist of large scale parallel computations of many grains to gain an understanding of the collective deformation behavior of groups of grains and to investigate the effects that grain size distribution has on these materials.

Acknowledgements

This work was performed under the auspices of NSF-Nanoscale Interdisciplinary Research Team under contract DMR-0210215 and ARL-Center for Advanced Materials and Ceramic Systems under the ARMAC-RTP Cooperative Agreement Number DAAD19-01-2-0003.

References

Anand, L., Kothari, M., 1996. A computational procedure for rate-independent crystal plasticity. Journal of the Mechanics and Physics of Solids 44 (4), 525–558.

Asaro, R.J., Krysl, P., Kad, B., 2003. Deformation mechanism transitions in nanoscale fcc metals. Philosophical Magazine Letters 83 (12), 733–743.

Asaro, R.J., Needleman, A., 1985. Overview no. 42 texture development and strain hardening in rate dependent polycrystals. Acta Metallurgica 33 (6), 923–953.

Ashby, M.F., Verrall, R.A., 1973. Diffusion-accommodated flow and super-plasticity. Acta Metallurgica 21 (2), 149–163.

Bathe, K.-J., Wilson, E.L., 1976. Numerical Methods in Finite Element Analysis. Prentice-Hall, Englewood Cliffs, NJ.

Capolungo, L., Jochum, C., Cherkaoui, M., Qu, J., 2005. Homogenization method for strength and inelastic behavior of nanocrystalline materials. International Journal of Plasticity 21 (1), 67–82.

Chen, M., Ma, E., Hemker, K.J., Sheng, H., Wang, Y., Cheng, X., 2003. Deformation twinning in nanocrystalline aluminum. Science 300 (5623), 1275–1277.

Coble, R.L., 1963. A model for boundary diffusion controlled creep in poly-crystalline materials. Journal of Applied Physics 34, 1979–1982.

Conrad, H., Narayan, J., 2000. On the grain size softening in nanocrystalline materials. Scripta Materialia 42 (11), 1025–1030.

Dalla Torre, F., Victoria, M., Van Swygenhoven, H., 2002. Nanocrystalline electrodeposited ni: microstructure and tensile properties. Acta Materialia 50 (15), 3957–3970.

Ebrahimi, F., Bourne, G., Kelly, M., Matthews, T., 1999. Mechanical properties of nanocrystalline nickel produced by electrodeposition. Nanostructured Materials 11 (3), 343–350.

Foiles, S.M., Baskes, M.I., Daw, M.S., 1986. Embedded-atom-method functions for the fcc metals cu, ag, au, ni, pd, pt, and their alloys. Physical Review B (Condensed Matter and Materials Physics) 33, 7983–7991.

Fu, H.-H., Benson, D., Meyers, M., 2001. Analytical and computational description of effect of grain size on yield stress of metals. Acta Materialia 49 (13), 2567–2582.

Fu, H.-H., Benson, D.J., Meyers, M.A., 2004. Computational description of nanocrystalline deformation based on crystal plasticity. Acta Materialia 52 (15), 4413–4425.

Gertsman, V., Hoffmann, M., Gleiter, H., Birringer, R., 1994. Study of grain size dependence of yield stress of copper for a wide grain size range. Acta Metallurgica et Materialia 42 (10), 3539–3544.

Gross, D., Li, M., 2002. Constructing microstructures of poly- and nanocrystalline materials for numerical modeling and simulation. Applied Physics Letters 80 (5), 746.

Hall, E., 1951. Deformation and ageing of mild steel. Physical Society – Proceedings 64 (381B), 747–753.

Hanyu, S., Nishimura, H., Matsunaga, K., Yamamoto, T., Ikuhara, Y., Sakuma, T., 2004. High temperature deformation behavior of [0 0 0 1] symmetrical tilt sigma 7 and sigma 21 grain boundaries in alumina bicrystals. Materials Transactions 45 (7), 2122–2127.

Hasnaoui, A., Van Swygenhoven, H., Derlet, P., 2003. Dimples on nanocrystalline fracture surfaces as evidence for shear plane formation. Science 300 (5625), 1550–1552.

Herring, C., 1950. Diffusional viscosity of polycrystalline solid. Journal of Applied Physics 21 (5), 437–445.

Horstemeyer, M., Baskes, M., Prantil, V., Philliber, J., Vonderheide, S., 2003. A multiscale analysis of fixed-end simple shear using molecular dynamics, crystal plasticity, and a macroscopic internal state variable theory. Modelling and Simulation in Materials Science and Engineering 11 (3), 265–286.

Hughes, J., 1987. The Finite Element Method. Dover, Mineola, New York.

Karimpoor, A., Erb, U., Aust, K., Palumbo, G., 2003. High strength nanocrystalline cobalt with high tensile ductility. Scripta Materialia 49 (7), 651–656.

Khan, A.S., Zhang, H., Takacs, L., 2000. Mechanical response and modeling of fully compacted nanocrystalline iron and copper. International Journal of Plasticity 16 (12), 1459–1476.

Kim, H., Estrin, Y., Bush, M., 2001. Constitutive modelling of strength and plasticity of nanocrystalline metallic materials. Materials Science and Engineering A 316 (1–2), 195–199.

Kumar, K., Van Swygenhoven, H., Suresh, S., 2003. Mechanical behavior of nanocrystalline metals and alloys. Acta Materialia 51 (19), 5743–5774.

Legros, M., Elliott, B., Rittner, M., Weertman, J., Hemker, K., 2000. Microsample tensile testing of nanocrystalline metals. Philosophical Magazine A: Physics of Condensed Matter, Structure, Defects and Mechanical Properties 80 (4), 1017–1026.

Liao, X., Zhao, Y., Srinivasan, S., Zhu, Y., Valiev, R., Gunderov, D., 2004. Deformation twinning in nanocrystalline copper at room temperature and low strain rate. Applied Physics Letters 84 (4), 592–594.

Miller, R.E., Tadmor, E., 2002. The quasicontinuum method: overview, applications and current directions. Journal of Computer-Aided Materials Design 9 (3), 203–239.

Nguyen, O., Ortiz, M., 2002. Coarse-graining and renormalization of atomistic binding relations and universal macroscopic cohesive behavior. Journal of the Mechanics and Physics of Solids 50 (8), 1727–1741.

Petch, N., 1953. The cleavage strength of polycrystals. Journal Iron Steel Institute 174, 25–28.

Rice, J., 1992. Dislocation nucleation from a crack tip. An analysis based on the peierls concept. Journal of the Mechanics and Physics of Solids 40 (2), 239.

Rice, J.R., Beltz, G.E., 1994. Activation energy for dislocation nucleation at a crack. Journal of the Mechanics and Physics of Solids 42 (2), 333–360.

Roundy, D., Krenn, C., Cohen, M.L., Morris, J.J., 1999. Ideal shear strengths of fcc aluminum and copper. Physical Review Letters 82 (13), 2713–2716.

Sanders, P., Eastman, J., Weertman, J., 1997. Elastic and tensile behavior of nanocrystalline copper and palladium. Acta Materialia 45 (10), 4019–4025.

Sansoz, F., Molinari, J., 2005. Mechanical behavior of [sigma] tilt grain boundaries in nanoscale cu and al: a quasicontinuum study. Acta Materialia 53 (7), 1931–1944.

Sansoz, F., Molinari, J.F., 2004. Incidence of atom shuffling on the shear and decohesion behavior of a symmetric tilt grain boundary in copper. Scripta Materialia 50 (10), 1283–1288.

Schiotz, J., Di Tolla, D., Jacobsen, K., 1998. Softening of nanocrystalline metals at very small grain sizes. Nature 391, 561–563.

Schiotz, J., Jacobsen, K.W., 2003. A maximum in the strength of nanocrystalline copper. Science 301 (5638), 1357–1359.

Schiotz, J., Vegge, T., Di Tolla, D., Jacobsen, K., 1999. Atomic-scale simulations of the mechanical deformation of nanocrystalline metals. Physical Review B (Condensed Matter and Materials Physics) 60, 971–983.

Schwaiger, R., Moser, B., Dao, M., Chollacoop, N., Suresh, S., 2003. Some critical experiments on the strain-rate sensitivity of nanocrystalline nickel. Acta Materialia 51 (17), 5159–5172.

Shan, Z., Stach, E.A., Wiezorek, J.M.K., Knapp, J.A., Follstaedt, D.M., Mao, S.X., 2004. Grain boundary-mediated plasticity in nanocrystalline nickel. Science 305 (5684), 654–657.

Shenoy, V., Miller, R., Tadmor, E., Rodney, D., Phillips, R., Ortiz, M., 1999. Adaptive finite element approach to atomic-scale mechanics – the quasicontinuum method. Journal of the Mechanics and Physics of Solids 47 (3), 611–642.

Spearot, D.E., Jacob, K.I., McDowell, D.L., 2004. Non-local separation constitutive laws for interfaces and their relation to nanoscale simulations. Mechanics of Materials 36 (9), 825–847.

Tadmor, E.B., Ortiz, M., Phillips, R., 1996. Quasicontinuum analysis of defects in solids. Philosophical Magazine A: Physics of Condensed Matter, Defects and Mechanical Properties 73 (6), 1529.

Van Swygenhoven, H., Derlet, P.M., 2001. Grain-boundary sliding in nanocrystalline fcc metals. Physical Review B (Condensed Matter and Materials Physics) 64 (22), 224105–224109.

Wang, Y., Wang, K., Pan, D., Lu, K., Hemker, K., Ma, E., 2003. Microsample tensile testing of nanocrystalline copper. Scripta Materialia 48 (12), 1581–1586.

Warner, D.H., Molinari, J.F., to be submitted. A multibody interface algorithm. International Journal of Numerical Methods in Engineering.

Wei, Q., Cheng, S., Ramesh, K.T., Ma, E., 2004. Effect of nanocrystalline and ultrafine grain sizes on the strain rate sensitivity and activation volume: fcc versus bcc metals. Materials Science and Engineering A 381 (1–2), 71–79.

Wei, Y.J., Anand, L., 2004. Grain-boundary sliding and separation in poly-crystalline metals: application to nanocrystalline fcc metals. Journal of the Mechanics and Physics of Solids 52 (11), 2587–2616.

Youngdahl, C.J., Sanders, P.G., Eastman, J.A., Weertman, J.R., 1997. Compressive yield strengths of nanocrystalline cu and pd. Scripta Materialia 37 (6), 809–813.